RSC Advances

PAPER

View Article Online
View Journal | View Issue

Cite this: *RSC Adv.*, 2021, **11**, 22826

One-step green synthesis of 2D Ag-dendrite-embedded biopolymer hydrogel beads as a catalytic reactor†

Jae Hwan Jeong,[a] Hee-Chul Woo[b] and Mun Ho Kim *[a]

Received 6th May 2021
Accepted 24th June 2021

DOI: 10.1039/d1ra03536c

rsc.li/rsc-advances

Silver (Ag) nanocrystals with a dendritic structure have attracted intensive attention because of their unique structural properties, which include abundant sharp corners and edges that provide a large number of active atoms. However, the synthesis of Ag dendrites *via* a simple and environmentally friendly method under ambient conditions remains a challenge. In this paper, we report a simple water-based green method for the production of biopolymer hydrogel beads embedded with Ag dendrites without using an additional reducing agent, stabilizer, or crosslinking agent. The obtained Ag dendrites exhibit a unique two-dimensional (2D) structure rather than a conventional three-dimensional structure because Ag^+ ions are reduced on the surface of the solid-phase hydrogel beads and grow into crystals. Reasonable mechanisms explaining the formation of the nanocomposite hydrogel beads and the formation of 2D Ag dendrites in the hydrogel are proposed on the basis of our observations and results. The hydrogel beads embedded the 2D Ag dendrites were used as an environmentally friendly catalytic reactor, and their catalytic performance was evaluated by adopting the reduction of 4-nitrophenol to 4-aminophenol with $NaBH_4$ as a model reaction.

1. Introduction

Hydrogels are crosslinked three-dimensional (3D) networks of hydrophilic polymer chains that can reversibly swell and de-swell in water.[1] Hydrogels, which can absorb a substantial amount of water or biological fluids, are soft and flexible and have thus have been used as biomaterials with tunable degradability for growing tissues and cells.[2] Incorporating metal nanocrystals into hydrogel networks can result in functional hydrogels with new chemical, physical, electrical, and mechanical properties,[3–8] extending their applications to include soft electronics, sensors, and catalysts.[9–13] Two synthetic approaches can be used to fabricate such novel hybrid materials: *ex situ* and *in situ* methods.[14] The *ex situ* method involves first forming metal nanocrystals and then injecting and dispersing them into a hydrogel. By contrast, in the *in situ* method, metal precursors are dissolved in a polymerizing or polymer solution for hydrogel formation and are then reduced to form metal nanocrystals inside the hydrogel. Between these methods, the *in situ* method is preferred because the *ex situ* method requires a relatively long processing time and continuous effort.[15] However, the *in situ* synthesis of hydrogels embedded with metal nanocrystals remains a challenge and is thus a topic of great interest.

Because the physical and chemical properties of noble-metal nanocrystals are strongly dependent on their shape and size, the shape- and size-controlled synthesis of noble-metal nanocrystals is an important topic.[16] Several synthesis methods that can produce various noble-metal structures such as nanospheres, nanoplates, nanocubes, and nanowires have been reported.[17–20] Among the prepared structures, dendritic structures of noble-metal nanocrystals have attracted intensive attention because of their unique structures, which include abundant sharp corners and edges that provide a large number of active atoms; these materials have thus been successfully used in catalysis, surface-enhanced Raman scattering (SERS), surface-enhanced fluorescence, and sensing applications.[21–28]

Several methods have been developed to synthesize these noble-metal nanocrystals with dendritic structures, including electrochemical deposition, electroless redox reactions, photochemical reduction, a sonoelectrochemical method, and a microwave-assisted solution method.[29–38] However, most of these methods require expensive and/or sophisticated equipment, a long reaction time, an elevated reaction temperature, complex synthesis steps, specific additives such as surfactants, and a supplementary etching process to remove the templates or surfactants.[39,40] Therefore, synthesizing Ag dendrites through a simple synthetic method without surfactants or harmful materials and under ambient conditions remains a challenge.

[a]*Department of Polymer Engineering, Pukyong National Univeristy, 45 Yongso-ro, Nam-gu, Busan 48513, Republic of Korea. E-mail: munho@pknu.ac.kr*

[b]*Department of Chemical Engineering, Pukyong National University, 45 Yongso-ro, Nam-gu, Busan 48513, Republic of Korea*

† Electronic supplementary information (ESI) available. See DOI: 10.1039/d1ra03536c

In the present paper, we report a simple, cost-effective, water-based green method for producing biopolymer hydrogel beads embedded with two-dimensional (2D) Ag dendrites. This new synthesis method was found to be a one-step protocol based on the *in situ* method, where an aqueous biopolymer solution is simply added into an aqueous metal precursor solution. In our investigations, without an additional reducing agent, stabilizer, or crosslinking agent, the biopolymer was crosslinked by the metal precursor ions and the metal precursor was subsequently reduced by the biopolymer under UV-light irradiation, resulting in the formation of hydrogel beads that contain uniformly embedded 2D Ag dendrites in a single step. The synthesis results were easy to reproduce, no special equipment was required for the synthesis, and the reaction was completed within 3 h. In particular, because the hydrogels are based on sodium alginate (a natural biopolymer extracted from brown seaweeds) and contain no organic material, they are environmentally friendly and safe to use and handle.

Surprisingly, Ag 2D dendrites, which have proven difficult to synthesize in wet chemical systems, can be prepared *via* our water-based one-step process at room temperature without any special surfactant or sophisticated equipment. We speculate that that the nonequilibrium synthesis conditions in which Ag^+ ions are reduced on the surface of the solid-phase hydrogel under exposure to UV light play a critical role. Reasonable mechanisms explaining the formation of the nanocomposite hydrogel beads and the formation of 2D Ag dendrites in the hydrogel are proposed on the basis of our observations and results. We used the hydrogel beads embedded with 2D Ag dendrites as a catalytic reactor for the reduction of 4-nitrophenol (4-NP) to 4-aminophenol (4-AP) in the presence of sodium borohydride ($NaBH_4$). The nanocomposite-hydrogel-based catalytic reactors showed excellent catalytic activity and could be reused several times without loss of activity.

2. Experimental

2.1 Chemicals and materials

Silver nitrate ($AgNO_3$), alginic acid sodium salt from brown algae (Na-alginate), $NaBH_4$, and 4-NP were products of Sigma-Aldrich and were used as received, without further purification. Deionized (DI) water was used in all reactions.

2.2 Synthesis of alginate beads embedded with 2D Ag dendrites

In this study, alginate beads embedded with 2D Ag dendrites were prepared by immersing aqueous alginate droplets in an aqueous $AgNO_3$ solution without adding an extra cross-linking agent for forming alginate hydrogels or an additional reducing agent for reducing the Ag^+ ions. Two hundred milligrams of Na-alginate were dissolved in 10 mL of deionized water, and 2 mL of the resultant aqueous alginate solution was loaded into a syringe and then dropped into a 0.125 M $AgNO_3$ aqueous solution at a rate of 10 mL h^{-1} using a syringe pump, producing alginate hydrogel beads cross-linked with Ag^+ ions. The aqueous solution containing alginate beads was aged for 3 h at room temperature under ultraviolet (UV) irradiation. The UV irradiation was applied using a UV curing lamp, and the output power of the UVA band (mainly 365 nm) was adjusted to 3.0 W cm^{-2}. During the UV irradiation, the aqueous solution containing alginate beads was shaken at intervals of 30 minutes to uniformly synthesize Ag nanocrystals on the entire surface of the beads. After 3 h, the prepared alginate beads were washed three times with DI water to remove the Ag^+ precursor remaining on the bead surface. After washing, the beads were stored in a dark room.

2.3 Catalytic activity

The catalytic reduction reaction was carried out using a 4.5 mL quartz cuvette with a 1 cm path length. Initially, an aqueous solution of 4-NP (5 μL, 280 mM) was prepared and added to a cuvette containing 1.2 mL of water. After $NaBH_4$ aqueous solution (0.2 mL, 700 mM) was added to the reactor, the 4-NP was converted to 1,4-nitrophenolate ion. Alginate beads embedded with 2D Ag dendrites were subsequently added to the reactor, and the UV-Vis absorption spectrum was recorded every 1 min.

2.4 Characterizations

The size, structure, and crystallinity of Ag nanocrystals were determined by a transmission electron microscopy (TEM). TEM images were taken with a HITACHI transmission electron microscope operated at an acceleration voltage of 80 kV. Samples for TEM observation were prepared by breaking the prepared alginate beads embedded with 2D Ag dendrites. About 10 as-prepared hybrid beads were placed in vial and 3 mL of DI water was added. The hydrogel beads were broken through the mechanical stirring (magnetic stirring at 1800 rpm) for 1 h. The hydrogel was selectively separated by means of centrifugation (6000 rpm for 8 min). After that, one drop of the remaining solution containing Ag nanocrystals was placed onto a carbon-coated copper grid and dried at room temperature prior to observation. High-resolution TEM images of Ag nanocrystals were taken using a Philips Tecnai F30 microscope operated at 300 kV. UV-Vis spectra were acquired at room temperature using a Cary 50 UV-Vis spectrophotometer (Agilent Technologies, USA). Thermogravimetric analysis (TGA) was conducted using a Pyris 1 thermogravimetric analyzer (Perkin-Elmer). X-ray photoelectron spectroscopy (XPS) was carried out using an Axis Nova spectrometer (Kartos Axis Nova, UK). Attenuated total reflectance Fourier transform infrared (ATR-FTIR) spectroscopy was conducted in the wavelength range from 500 to 4000 cm^{-1} using a model 5700 (Thermo Nicolet) attenuated total reflectance Fourier transform infrared spectrometer.

3. Results and discussion

3.1 One-step synthesis of alginate hydrogel beads embedded with 2D Ag dendrites

To synthesize alginate beads embedded with Ag nanocrystals, a single-step-based *in situ* crosslinking and reduction method was used. In this method, droplets of aqueous alginate solution

were dropped into a 0.125 M aqueous $AgNO_3$ solution. Fig. 1(a) shows a photograph of the sample prepared immediately after dropping, which indicates that the alginate chains could be crosslinked by Ag^+ ions to form a bead shape. Ionic crosslinking of alginate is well known to occur when guluronic acid (G-block) groups in different alginate chains are bonded *via* multivalent cations.[41] However, the results in Fig. 1(a) indicate that alginate chains can be ionically crosslinked in the presence of monovalent cations such as Ag^+. To confirm the gelation of Na-alginate by Ag^+ ions, droplets of Na-alginate aqueous solution containing Au nanocrystals (used as pigment) were formed and then immersed in an $AgNO_3$ aqueous solution and in pure water. As shown in Fig. S1,† the alginate droplets containing Au nanocrystals immersed in an aqueous solution containing 0.125 M $AgNO_3$ were cross-linked and maintained the spherical shape of the original droplets. By contrast, the droplets immersed in pure water collapsed and the Au nanocrystals were dispersed in the entire medium (Fig. S1†). These results clearly demonstrate that alginate chains can be ionically crosslinked in the presence of Ag^+.

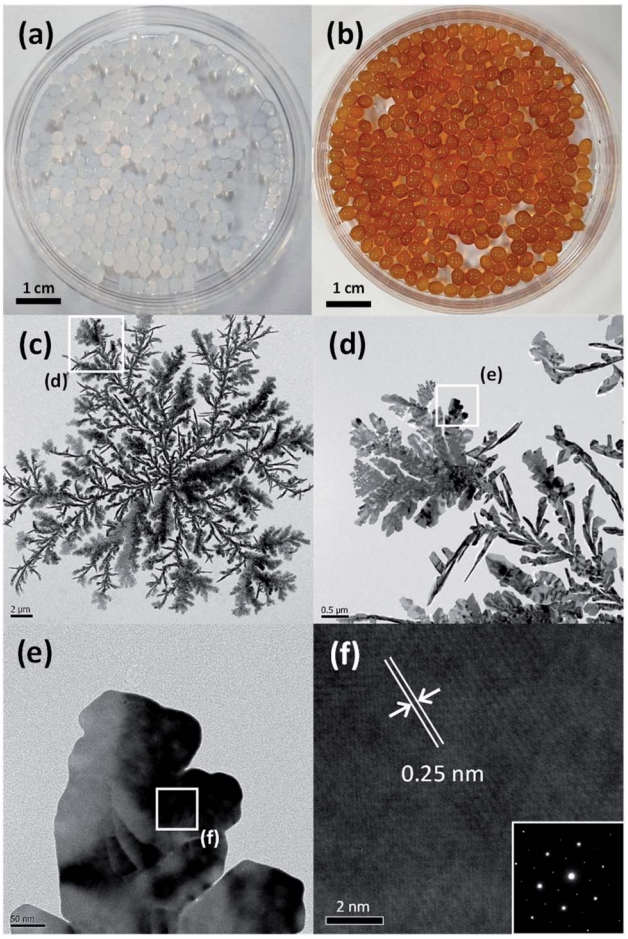

Fig. 1 Photographs of (a) alginate beads formed by immersion in 0.125 M $AgNO_3$ aqueous solution and (b) alginate beads obtained after immersing in 0.125 M $AgNO_3$ and aging at room temperature for 3 h under UV irradiation. (c) TEM image of an Ag dendrite formed in the alginate beads. (d–f) HR-TEM images of the Ag dendrite. The inset in (f) shows the fast Fourier transform (FFT) of the image.

The 0.125 M $AgNO_3$ aqueous solution where the alginate hydrogel beads were formed was aged under UV irradiation at room temperature During the UV irradiation, the aqueous solution containing alginate beads was shaken at intervals of 30 minutes to uniformly synthesize Ag nanocrystals on the entire surface of the beads. The beads, which were initially translucent, turned brown after the UV irradiation for 3 h (Fig. 1(b)). This color change indicates that Ag^+ ions were reduced and Ag nanocrystals were formed during the aging process, and, thus, that alginate beads embedded with Ag nanocrystals were formed. To examine the shape of the formed Ag nanocrystals, the alginate beads embedded with Ag nanocrystals were mechanically destroyed and the Ag nanocrystals were collected through a centrifugation process. Fig. 1(c) shows a TEM image of the obtained Ag nanocrystals, indicating that the Ag nanocrystals formed in the alginate beads exhibited a two-dimensional (2D) dendrite shape. Several branches grew radially from the center and were further divided into sub-branches. The diameter of the 2D Ag dendrite shown in Fig. 1(c) was approximately 24.6 μm. Fig. 1(d)–(f) shows high-resolution (HR) TEM images of the 2D Ag dendrite. The lattice fringes indexed in the HR-TEM image in Fig. 1(f) confirm the crystallinity of the Ag dendrite; the measured lattice spacing of 0.25 nm corresponds to the 1/3{422} reflection that is generally forbidden for a face-centered cubic lattice.[42] This forbidden reflection has been previously observed for Ag nanostructures in the form of thin plates.[43] The inset in Fig. 1(f) shows the fast Fourier transform (FFT) pattern of a high-resolution TEM image. The diffraction spots with six-fold rotational symmetry imply that the plane is bounded by the {111} plane.[44] The XPS analysis results for the 2D dendrite are shown in Fig. 2(a), and the asymmetric spectra for the Ag 3d line confirm that the Ag was present only in the zero-valent state.[45] These results indicate that alginate beads embedded with 2D Ag dendrites can be prepared by simply adding aqueous Na-alginate droplets to an $AgNO_3$ aqueous solution and then exposing the mixture to UV light. We used TGA to determine the mass of the Ag nanocrystals in the beads shown in Fig. 1(b). The results show that the Ag nanocrystals composed approximately 49.4 wt% of the bead mass in the dried state (Fig. 2(b)).

In this method, alginate acted as a reducing agent; however, UV light was also found to strongly affect the formation of Ag nanocrystals. The formation of Ag nanocrystals in the alginate beads was considerably influenced by the light intensity depending on the type of light source. In the above experiments, UV irradiation was conducted *via* a UV curing lamp with a substantial ultraviolet energy. In the experiment conducted under the identical conditions in a dark room, alginate beads did not exhibit a color change, maintaining their initial translucent color; this observation indicates that Ag nanocrystals were not formed in the alginate beads in the absence of UV light (Fig. S2(a)†). When the beads were exposed to sunlight instead of UV light, the color changed to bright-yellow, indicating that Ag nanocrystals were formed but not in large quantities (Fig. S2(b)†). Fig. S2(c) and (d)† shows photographs of beads fabricated without stirring using a Xe lamp that produces light of relatively lower ultraviolet energy than a UV lamp under the

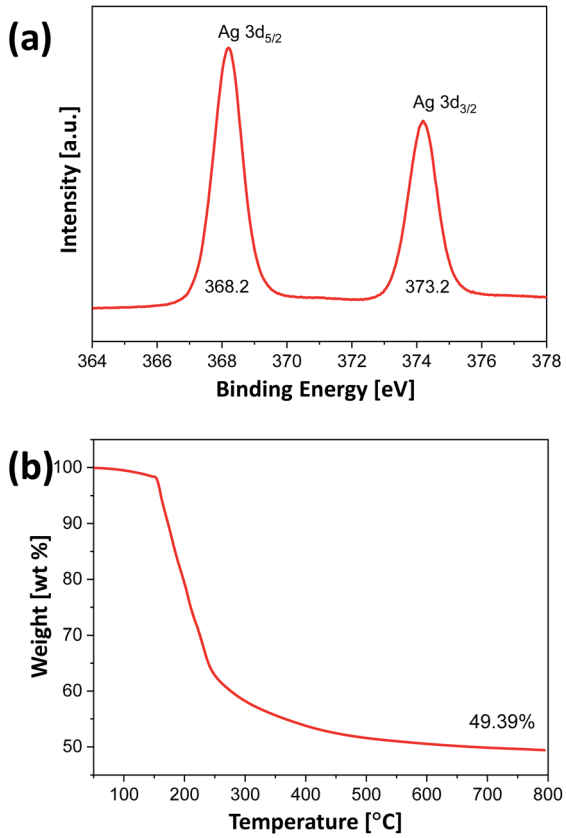

Fig. 2 (a) High-resolution XPS Ag 3d peaks and (b) TGA data for alginate beads embedded with 2D Ag dendrites, after the complete drying of water.

identical conditions. As shown in the figure, one side of the beads exposed to light turned brown, confirming that Ag crystals were selectively formed only in the area exposed to light (Fig. S2(c) and (d)†). Fig. S2(e) and (f)† show TEM images of Ag nanocrystals obtained by using the Xe lamp, which were quite different from the TEM images shown in Fig. 1. When the $AgNO_3$ aqueous solution not containing Na-alginate was exposed to UV light, the solution did not show any color change, indicating that Ag nanocrystals were not formed in the absence of alginate. Collectively, these results indicate that Ag nanocrystals were formed when both alginate and UV light were present, and Ag nanocrystals having dendritic structures were formed in 3 h under UV irradiation with a substantial ultraviolet energy.

Alginate is an anionic polymer with a high charge density, and their negative charge character promotes the attraction of Ag^+ ions to the polymer chains (the carboxyl groups) in an aqueous $AgNO_3$ solution.[46] The alginate chains can then be ionically crosslinked by the Ag^+ ions, and some of the Ag^+ ions can be reduced by the adjacent hydroxyl groups of alginate under UV irradiation.[47,48] The reduced Ag atoms coalesce, leading to the formation of metal clusters, and continue to grow into nanocrystals. Fig. S3† shows the FTIR spectrum of Na-alginate and alginate beads immersed in 0.125 M $AgNO_3$ aqueous solution for 3 h under UV irradiation. In the spectrum

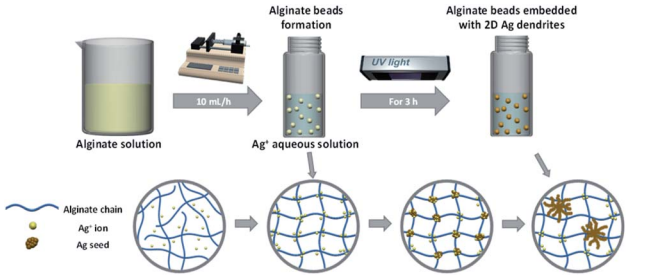

Fig. 3 Schematic of the proposed *in situ* synthesis process of alginate hydrogel beads embedded with 2D Ag dendrites.

of pure Na-alginate, the absorption band of 3254 cm^{-1} is assigned to hydroxyl groups, and the absorption peaks at 1595 and 1407 cm^{-1} are due to the asymmetric and symmetric elongation vibrations of carboxyl groups, respectively.[49] Interestingly, after the ion exchange and reduction of Ag^+ ions, the peaks at 1595 and 1407 cm^{-1} shifted to 1574 and 1393 cm^{-1}, respectively, clearly indicating that the carboxyl groups in the alginate interacted with Ag^+ ions.[50] On the basis of these results, we concluded that alginate beads embedded with 2D Ag dendrites can be prepared *in situ* by simply immersing droplets of an alginate aqueous solution in a $AgNO_3$ aqueous solution, followed by UV irradiation. Fig. 3 shows a schematic of the *in situ* synthesis process of alginate hydrogel beads embedded with 2D Ag dendrites proposed in the present study.

3.2 Growth mechanism of 2D Ag dendrites

The Ag dendrites obtained in the present study showed distinctly different features than the dendrites synthesized in previous related studies. Specifically, they exhibit a 2D structure, whereas most of the dendrites reported in the previous studies were 3D. In the present study, because the Ag nanocrystals are mainly generated and grown on the surface of the alginate hydrogel beads exposed to UV light, they are expected to have a 2D structure instead of the 3D structures generated in homogeneous solutions. To observe the growth behavior of the Ag nanocrystals with the 2D dendrite structure, we used TEM to observe the morphologies of Ag nanocrystals prepared under identical conditions but with the reaction time varied; the results are shown in Fig. 4. In the early stage of the reaction, Ag nanocrystals grew, forming particles in the form of thin plates (Fig. 4(a)). After 10 min, clusters of plates with several branches (dendrite embryo) were formed, as shown in Fig. 4(b), and an imperfect dendrite-like structure with new branches was formed after 30 min of reaction (Fig. 4(c)). As the reaction time increased, the branches continued to grow and new sub-branches began to form, resulting in a structure resembling a dendritic structure; the particle size gradually increased (Fig. 4(d) and (e)). When the reaction time was increased to 3 h, a large number of dense sub-branches were formed and the branches became thicker, resulting in a highly branched dendrite structure larger than 24 μm (Fig. 4(f)).

The formation and growth of 2D Ag dendrites can be explained by the following mechanism. As shown in Fig. 4(a), Ag

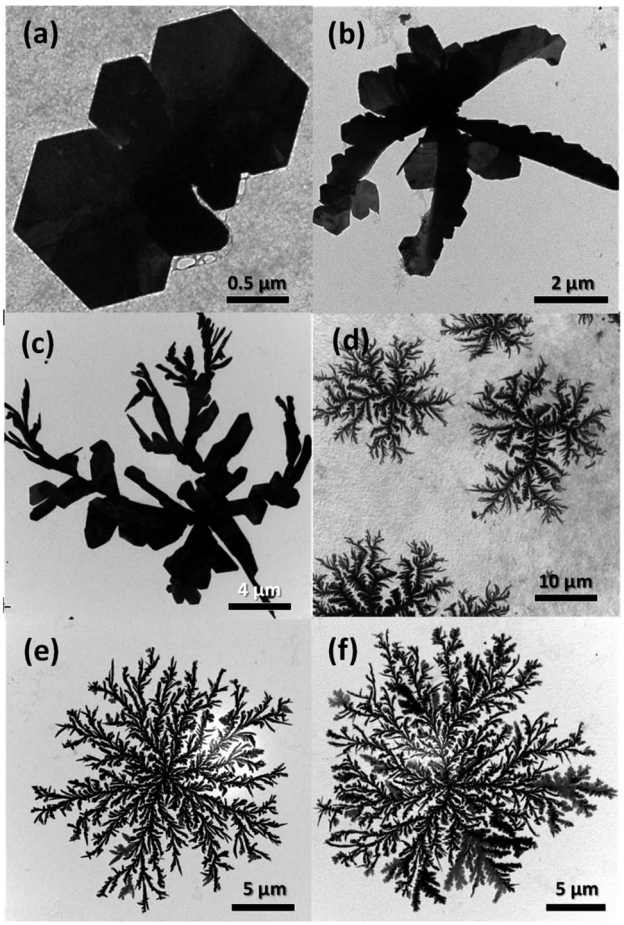

Fig. 4 TEM images of the products sampled at different stages of the reaction: (a) 5 min, (b) 10 min, (c) 30 min, (d) 1 h, (e) 2 h, and (f) 3 h.

nanoplates were formed at the beginning of the reaction; nanoplates have frequently been observed when such anisotropic nanostructures have been formed using a reducing agent with mild reducing power. For the shape-controlled synthesis of Ag nanocrystals, precisely controlling the reduction kinetics of Ag^+ ions is important. The total free energy of Ag nanoplates is high because the surface area is relatively large and the lattice strain energy due to defects is high.[51] Therefore, the formation of nanoplates is not thermodynamically favored, and nanoplate structures can only be obtained by inducing reactions under kinetically controlled conditions.[52] Specifically, when the reduction rate of Ag^+ ions is low, the formation of nanocrystals is governed by reaction kinetics, not thermodynamics; thus, anisotropic nanostructures such as nanoplates can be formed.[53] Because the reducing power of alginate (the reductant in the present study) at room temperature is low, Ag nanoplates were formed at the beginning of the reaction. The dendrite embryo shown in Fig. 4(b) was asymmetric and irregular in shape but uniform in thickness. These structural characteristics indicate that the structure was unlikely to have been produced through the growth process associated with conventional nucleation and Ostwald ripening.[54] We speculated that the nanoplates initially formed under kinetic control were fused together along their side planes *via* the mechanism of oriented attachment to form a secondary cluster structure of nanoplates, as shown in Fig. 4(b).[55]

The dendrite structure is generally acknowledged to form through anisotropic crystal growth of nanocrystals in a nonequilibrium state in which the kinetic factor dominates the thermodynamic factor.[56–58] Such conditions are difficult to achieve in homogeneous solutions based on wet chemical synthesis.[39] However, when the reaction occurs at the interface of a solid-phase reducing agent, the nonequilibrium conditions are easily realized.[59] In the present study, the solid-phase alginate hydrogel beads acted as the reducing agent and Ag atoms were generated on the surface of the alginate hydrogel beads irradiated with UV light. After the dendrite embryos (Fig. 4(b)) had formed, Ag^+ ions in the aqueous solution continued to diffuse into the beads and were reduced in the surface of the beads under UV irradiation. The Ag atoms then agglomerated and grew into small Ag clusters, and alginate served as a colloidal stabilizer for these clusters. However, because alginate in this state was crosslinked, the movement and growth of the small Ag clusters stabilized by alginate was retarded by the polymer network. The Ag clusters then underwent a random walk and combined with the existing seed particles, forming fractal dendritic structures (Fig. 4(c)–(d)); this process is described by the diffusion-limited aggregation model.[60] When the dendrite structures formed, the particles appeared to grow through Ostwald ripening with diminishing small particles and the number and width of branches in the dendrites increased with increasing reaction time (Fig. 4(e) and (f)).

Fig. 5 shows TEM images of Ag nanocrystals prepared using various concentrations of $AgNO_3$ in the aqueous solutions to

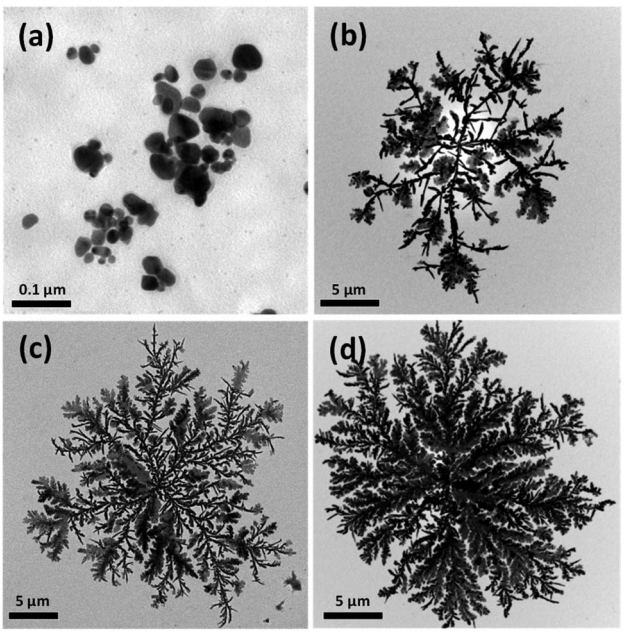

Fig. 5 TEM images of 2D Ag dendrites prepared using various concentrations of the Ag precursor. The concentrations of Ag^+ ions were (a) 30 mM, (b) 62.5 mM, (c) 0.125 M, and (d) 0.5 M.

which the alginate beads were added. In the present study, when the concentration of $AgNO_3$ was less than 60 mM, added alginate droplets were broken in the aqueous solution and the bead structures could not be formed, indicating that, when the concentration of Ag^+ ions was low, the polymer chains of alginate were not properly crosslinked and the hydrogel bead was not generated. Fig. 5(a) shows Ag nanocrystals synthesized in the solution in which alginate droplets were broken and uniformly dispersed, indicating that the Ag nanocrystals formed in the homogeneous solution state did not exhibit the dendritic shape. When the concentration of $AgNO_3$ was greater than 60 mM, alginate beads were formed and Ag nanocrystals synthesized on the beads formed dendrites (Fig. 5(b)–(d)). With increasing concentration of the $AgNO_3$ solution, the dendrites became larger and denser because more Ag^+ ions could be reduced and added to the dendrites. These results demonstrate that 2D dendritic metal structures can be efficiently formed when alginate hydrogel beads (as a solid-phase reducing agent) are formed and the reduction of Ag^+ ions and the crystal growth occur in the hydrogel beads.

3.3 Catalytic reactor based on alginate hydrogel embedded with 2D Ag dendrites

The use of water in catalytic reactions is one of the most powerful tools of green chemistry because it reduces pollution by reducing the release of toxic chemicals into the environment.[61] Hydrogels contain a large amount of water and, in their swollen state, exhibit a higher surface-area-to-volume ratio and greater porosity. This feature enables the efficient diffusion of reactive molecules in the water through the surface of the hydrogel, where they interact with the hydrogel substrates. This behavior is advantageous for a catalyst support material.[62] The literature includes various accounts of noble-metal nanocrystals exhibiting high activity and excellent selectivity as catalysts.[63,64] The alginate hydrogel beads embedded with 2D Ag dendrites synthesized in the present study can be used as ecofriendly heterogeneous catalysts because the 2D Ag dendrites were uniformly formed in the surface of the hydrogel beads, as previously described. Because the 2D Ag dendrites are embedded in the hydrogel, they should not degrade or aggregate when catalyzing a reaction. In addition, the large size of the beads enables their easy separation from the reaction mixture. Thus, the heterogeneous catalyst can be readily separated and reused after the reaction is completed.

To evaluate the catalytic performance of the hydrogel beads embedded with 2D Ag dendrites synthesized in the present study, the catalytic conversion of 4-NP to 4-AP in the presence of excess sodium borohydride ($NaBH_4$) was carried out as a model reaction. Fig. 6(a) shows the absorption spectra of 4-NP, 4-nitrophenolate ion, and 4-AP. The spectrum of 4-NP shows an absorption peak at 317 nm. When $NaBH_4$ was added to the 4-NP aqueous solution, the 4-NP was converted to 4-nitrophenolate and the peak of 4-NP at 317 nm correspondingly shifted to 398 nm.[65] The absorption peak of 4-AP was observed at 305 nm (Fig. 6(a)). 4-NP can be reduced to 4-AP using $NaBH_4$ as a reducing agent; however, this reaction is kinetically slow,

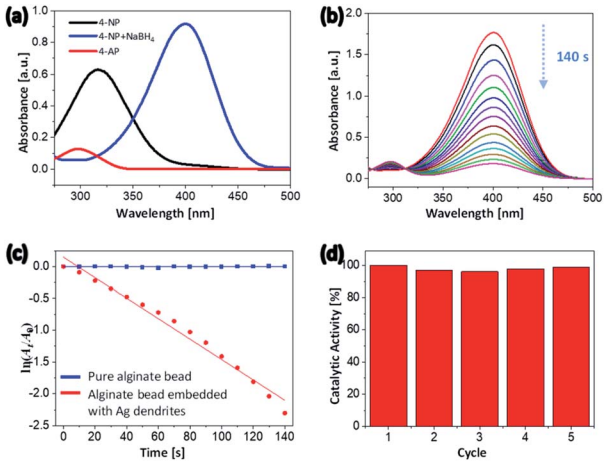

Fig. 6 (a) UV-Vis spectra of freshly prepared solutions of 4-NP, 4-NP mixed with $NaBH_4$, and 4-AP. (b) UV-Vis absorption spectra at various reaction times and (c) the linear fit of $\ln(A_t/A_0)$ *vs.* reaction time for the catalytic reduction of 4-NP with $NaBH_4$ in the presence of the hydrogel beads embedded with 2D Ag dendrites. (d) Recyclability of the hybrid hydrogel beads used as a catalytic reactor for the reduction of 4-NP with $NaBH_4$.

requiring a reaction time of a few days.[66] The addition of a small amount of catalyst shortens the reaction time to a few minutes. When $NaBH_4$ was not added, the peak in the UV-Vis absorption spectrum did not change over time because 4-NP could not be reduced to 4-AP. Fig. 6(b) shows the UV-Vis absorption spectra recorded at 10 s intervals after the hydrogel beads embedded with 2D Ag dendrites were added to the reaction mixture. The intensity of the 4-nitrophenolate peak at 398 nm gradually decreased with increasing reaction time; after 140 s, the peak had almost completely disappeared. In addition, the intensity of the absorption peak of 4-AP at 305 nm, which was initially close to 0, gradually increased with time, indicating that the reduction reaction proceeded. When an alginate hydrogel bead crosslinked with Ba^{2+} ions and not including Ag nanocrystals was used as a catalyst, the peak at 398 nm did not change for 10 min (Fig. S4†), indicating that the reduction reaction did not occur in the absence of the 2D Ag dendrites. Because the reduction rate does not depend on the concentration of $NaBH_4$ that is present in excess compared with 4-NP, the catalytic rate constant can be calculated using the first-order reaction equation. The plot of $\ln(A_t/A_0)$ *vs.* reaction time (Fig. 6(c)) shows a linear relationship, where A_t and A_0 are the absorbance at time t and at time zero, respectively. The rate constant of alginate beads with 2D Ag dendrites, which was calculated on the basis of the slope of the linear region of the plot, was 1.609×10^{-2} s^{-1}.

Catalyst recovery and reuse are an important consideration in modern catalysis.[67] Because the hydrogel beads with embedded 2D Ag dendrites synthesized in the present study exhibit a large particle size, the beads were easily removed from the reaction mixture after the catalytic reduction was completed, making them easy to reuse. In Fig. 6(d), the reusability of the catalytic reactors was assessed in experiments where the same hybrid hydrogel beads were used repeatedly. During five reuse cycles, the catalyst activity based on the

conversion percent of 4-NP was measured to be almost identical, demonstrating that the heterogeneous catalyst exhibited excellent reusability and good stability.

To quantitatively compare the catalytic activity of the hybrid hydrogel bead catalyst with that of other reported catalysts, we used the activity parameter $\kappa = k/m$, where k is the rate constant and m is the total mass of catalyst added in the reaction.[68] The κ value of the alginate beads embedded with 2D Ag dendrites was calculated to be 40.23 s^{-1} g^{-1}. As far as we know, this value is high among values reported for heterogeneous catalysts based on noble-metal nanoparticles (*e.g.*, Ag, Au, Pd, and Pt) used in the catalytic reduction of 4-NP to 4-AP by $NaBH_4$ (Table S1†). The improved activity of our system may be attributable to the unique structure of the 2D Ag dendrites because the dendrite structures have a high specific surface area with open pores and abundant sharp edges/corners. These results also confirm that the hydrogel beads with a high surface-area-to-volume ratio and high porosity in the swollen state in water can be used as excellent catalyst support materials.

4. Conclusions

Alginate hydrogel beads embedded with 2D Ag dendrites were synthesized by simply adding aqueous alginate droplets to an aqueous $AgNO_3$ solution. The alginate was crosslinked by Ag^+ ions, and the Ag^+ ions were reduced by alginate to form Ag nanocrystals with a dendritic shape, leading to the formation of the hydrogel beads embedded with 2D Ag dendrites. UV light strongly affected the reduction of Ag^+ ions. In the present study, because the reduction of Ag^+ ions occurred mainly on the surface of the alginate beads (as a solid-phase reductant), nonequilibrium conditions could be easily realized, which promoted the formation of Ag nanocrystals with a dendritic shape based on diffusion-limited aggregation. The hydrogel beads embedded with 2D Ag dendrites exhibited excellent catalytic activity and reusability when used as a catalytic reactor for the conversion of 4-NP to 4-AP by $NaBH_4$. This study demonstrates our ability to develop 2D Ag dendrites *via* a new chemical reduction system and also confirms the feasibility of using hydrogels as new support materials for developing catalytic reactors with excellent catalytic performance and reusability.

Author contributions

Jae Hwan Jeong: conceptualization, methodology, investigation, writing – original draft. Hee-Chul Woo: methodology, investigation, funding acquisition. Mun Ho Kim: conceptualization, methodology, validation, investigation, resource, writing – review & editing, supervision, project administration, funding acquisition.

Conflicts of interest

The authors declare that they have no known competing financial interests or personal relationships that could have appeared to influence the work reported in this paper.

Acknowledgements

This research was supported by the National Research Foundation of Korea (NRF) grant funded by the Korea government (MSIT) (No. 2021R1A2C1009832). This work was also supported by the Korea Institute of Energy Technology Evaluation and Planning (KETEP) and the Ministry of Trade, Industry & Energy (MOTIE) of the Republic of Korea (No. 20194010201840) and by the BB21plus funded by Busan Metropolitan City and Busan Institute for Talent & Lifelong Education (BIT).

References

1 F. Ullah, M. B. H. Othman, F. Javed, Z. Ahmad and H. M. Akil, Classification, processing and application of hydrogels: a review, *Mater. Sci. Eng., C*, 2015, **57**, 414–433.
2 E. Caló and V. V. Khutoryanskiy, Biomedical applications of hydrogels: a review of patents and commercial products, *Eur. Polym. J.*, 2015, **65**, 252–267.
3 S. Rafieian, H. Mirzadeh, H. Mahdavi and M. E. Masoumi, A review on nanocomposite hydrogels and their biomedical applications, *Sci. Eng. Compos. Mater.*, 2019, **26**, 154–174.
4 J. E. Song and E. C. Cho, Dual-responsive and multifunctional plasmonic hydrogel valves and biomimetic architectures formed with hydrogel and gold nanocolloids, *Sci. Rep.*, 2016, **6**, 34622.
5 F. Wahid, X. J. Zhao, S. R. Jia, H. Bai and C. Zhong, Nanocomposite hydrogels as multifunctional systems for biomedical applications: Current state and perspectives, *Composites, Part B*, 2020, **200**, 108208.
6 A. Choe, J. Yeom, R. Shanker, M. P. Kim, S. Kang and H. Ko, Stretchable and wearable colorimetric patches based on thermoresponsive plasmonic microgels embedded in a hydrogel film, *NPG Asia Mater.*, 2018, **10**, 912–922.
7 M. Zakia, J. M. Koo, D. Kim, K. Ji, P. H. Huh, J. Yoon and S. Il Yoo, Development of silver nanoparticle-based hydrogel composites for antimicrobial activity, *Green Chem. Lett. Rev.*, 2020, **13**, 34–40.
8 P. Thoniyot, M. J. Tan, A. A. Karim, D. J. Young and X. J. Loh, Nanoparticle–Hydrogel Composites: Concept, Design, and Applications of These Promising, Multi-Functional Materials, *Adv. Sci.*, 2015, **2**, 1400010.
9 Q. Mao, S. Shi and H. Wang, Biomimetic Nanowire Structured Hydrogels as Highly Active and Recyclable Catalyst Carriers, *ACS Sustainable Chem. Eng.*, 2015, **3**, 1915–1924.
10 Y. Zhou, C. Wan, Y. Yang, H. Yang, S. Wang, Z. Dai, K. Ji, H. Jiang, X. Chen and Y. Long, Highly Stretchable, Elastic, and Ionic Conductive Hydrogel for Artificial Soft Electronics, *Adv. Funct. Mater.*, 2019, **29**, 1–8.
11 S. H. Kim, H. C. Woo and M. H. Kim, Solid-phase colorimetric sensing probe for bromide based on a tough hydrogel embedded with silver nanoprisms, *Anal. Chim. Acta*, 2020, **1131**, 80–89.
12 C. Lim, Y. Shin, J. Jung, J. H. Kim, S. Lee and D. H. Kim, Stretchable conductive nanocomposite based on alginate

hydrogel and silver nanowires for wearable electronics, *APL Mater.*, 2019, **7**, 031502.
13 Z. Wang, Y. Cong and J. Fu, Stretchable and tough conductive hydrogels for flexible pressure and strain sensors, *J. Mater. Chem. B*, 2020, **8**, 3437–3459.
14 H. L. Tan, S. Y. Teow and J. Pushpamalar, Application of metal nanoparticle–hydrogel composites in tissue regeneration, *Bioengineering*, 2019, **6**, 1–17.
15 Y. J. Yang, M. H. Kim and O. O. Park, In situ synthesis of gold nanocrystal-embedded poly(dimethylsiloxane) films with nanostructured surface patterns, *Microelectron. Eng.*, 2017, **179**, 1–6.
16 Y. Xia, Y. Xiong, B. Lim and S. E. Skrabalak, Shape-controlled synthesis of metal nanocrystals: Simple chemistry meets complex physics?, *Angew. Chem., Int. Ed.*, 2009, **48**, 60–103.
17 M. H. Kim, X. Lu, B. Wiley, E. P. Lee and Y. Xia, Morphological evolution of single-crystal Ag nanospheres during the galvanic replacement reaction with $HAuCl_4$, *J. Phys. Chem. C*, 2008, **112**, 7872–7876.
18 Y. Yang, X. L. Zhong, Q. Zhang, L. G. Blackstad, Z. W. Fu, Z. Y. Li and D. Qin, The role of etching in the formation of ag nanoplates with straight, curved and wavy edges and comparison of their SERS properties, *Small*, 2014, **10**, 1430–1437.
19 S. H. Im, T. L. Yun, B. Wiley and Y. Xia, Large-scale synthesis of silver nanocubes: The role of HCl in promoting cube perfection and monodispersity, *Angew. Chem., Int. Ed.*, 2005, **44**, 2154–2157.
20 A. R. Rathmell and B. J. Wiley, The synthesis and coating of long, thin copper nanowires to make flexible, transparent conducting films on plastic substrates, *Adv. Mater.*, 2011, **23**, 4798–4803.
21 L. Fu, T. Tamanna, W. J. Hu and A. Yu, Chemical preparation and applications of silver dendrites, *Chem. Pap.*, 2014, **68**, 1283–1297.
22 S. Xie, X. Zhang, D. Xiao, M. C. Paau, J. Huang and M. M. F. Choi, Fast growth synthesis of silver dendrite crystals assisted by sulfate ion and its application for surface enhanced Raman scattering, *J. Phys. Chem. C*, 2011, **115**, 9943–9951.
23 F. Urbain, P. Tang, N. M. Carretero, T. Andreu, J. Arbiol and J. R. Morante, Tailoring copper foam with silver dendrite catalysts for highly selective carbon dioxide conversion into carbon monoxide, *ACS Appl. Mater. Interfaces*, 2018, **10**, 43650–43660.
24 M. H. Rashid and T. K. Mandal, Synthesis and catalytic application of nanostructured silver dendrites, *J. Phys. Chem. C*, 2007, **111**, 16750–16760.
25 L. Hu, Y. J. Liu, Y. Han, P. Chen, C. Zhang, C. Li, Z. Lu, D. Luo and S. Jiang, Graphene oxide-decorated silver dendrites for high-performance surface-enhanced Raman scattering applications, *J. Mater. Chem. C*, 2017, **5**, 3908–3915.
26 D. Ge, J. Wei, J. Ding, J. Zhang, C. Ma, M. Wang, L. Zhang and S. Zhu, Silver Nano-Dendrite-Plated Porous Silicon Substrates Formed by Single-Step Electrochemical Synthesis for Surface-Enhanced Raman Scattering, *ACS Appl. Nano Mater.*, 2020, **3**, 3011–3018.
27 J. Dong and H. Zheng, Self-assembled synthesis of SEF-active silver dendrites by galvanic displacement on copper substrate, *Appl. Phys. B: Lasers Opt.*, 2013, **111**, 523–526.
28 S. Dhanush, M. Sreejesh, K. Bindu, P. Chowdhury and H. S. Nagaraja, Synthesis and electrochemical properties of silver dendrites and silver dendrites/rGO composite for applications in paracetamol sensing, *Mater. Res. Bull.*, 2018, **100**, 295–301.
29 M. V. Mandke, S. H. Han and H. M. Pathan, Growth of silver dendritic nanostructures *via* electrochemical route, *CrystEngComm*, 2012, **14**, 86–89.
30 J. Li, W. Fa, H. Zhao, C. Zhu, H. Jia and L. Gu, Dendritic silver hierarchical structures for anode materials in Li ion batteries, *Micro Nano Lett.*, 2019, **14**, 887–891.
31 W. Ye, Y. Chen, F. Zhou, C. Wang and Y. Li, Fluoride-assisted galvanic replacement synthesis of Ag and Au dendrites on aluminum foil with enhanced SERS and catalytic activities, *J. Mater. Chem.*, 2012, **22**, 18327–18334.
32 D. Silver, N. Growth and R. Reaction, Dendritic Silver Nanostructure Growth and Evolution in Replacement Reaction, *Cryst. Growth Des.*, 2007, **7**, 864–867.
33 Z. Zhao, N. Chamele, M. Kozicki, Y. Yao and C. Wang, Photochemical synthesis of dendritic silver nano-particles for anti-counterfeiting, *J. Mater. Chem. C*, 2019, **7**, 6099–6104.
34 S. Gupta and R. Prakash, Photochemical assisted formation of silver nano dendrites and their application in amperometric sensing of nitrite, *RSC Adv.*, 2014, **4**, 7521–7527.
35 Q. Shen, L. Jiang, H. Zhang, Q. Min, W. Hou and J. J. Zhu, Three-dimensional dendritic Pt nanostructures: Sonoelectrochemical synthesis and electrochemical applications, *J. Phys. Chem. C*, 2008, **112**, 16385–16392.
36 I. Haas, S. Shanmugam and A. Gedanken, Synthesis of copper dendrite nanostructures by a sonoelectrochemical method, *Chem.–Eur. J.*, 2008, **14**, 4696–4703.
37 R. He, X. Qian, J. Yin and Z. Zhu, Formation of silver dendrites under microwave irradiation, *Chem. Phys. Lett.*, 2003, **369**, 454–458.
38 M. Noroozi, A. Zakaria, M. M. Moksin, Z. A. Wahab and A. Abedini, Green formation of spherical and dendritic silver nanostructures under microwave irradiation without reducing agent, *Int. J. Mol. Sci.*, 2012, **13**, 8086–8096.
39 S. R. Bahadori, L. Mei, A. Athavale, Y. J. Chiu, C. S. Pickering and Y. Hao, New Insight into Single-Crystal Silver Dendrite Formation and Growth Mechanisms, *Cryst. Growth Des.*, 2020, **20**, 7291–7299.
40 G. Zhang, S. Sun, M. N. Banis, R. Li, M. Cai and X. Sun, Morphology-controlled green synthesis of single crystalline silver dendrites, dendritic flowers, and rods, and their growth mechanism, *Cryst. Growth Des.*, 2011, **11**, 2493–2499.
41 S. H. Gwon, J. Yoon, H. K. Seok, K. H. Oh and J. Y. Sun, Gelation dynamics of ionically crosslinked alginate gel with various cations, *Macromol. Res.*, 2015, **23**, 1112–1116.
42 A. Pradyasti, D. H. Kim, M. N. Biutty, S. Il Yoo and M. H. Kim, Ag–Ag2S hybrid nanoplates with unique heterostructures:

Facile synthesis and photocatalytic application, *J. Alloys Compd.*, 2020, **826**, 154191.

43 M. R. Langille, M. L. Personick and C. A. Mirkin, Plasmon-mediated syntheses of metallic nanostructures, *Angew. Chem., Int. Ed.*, 2013, **52**, 13910–13940.

44 J. Kim, S. W. Lee, M. H. Kim and O. O. Park, Zigzag-Shaped Silver Nanoplates: Synthesis *via* Ostwald Ripening and Their Application in Highly Sensitive Strain Sensors, *ACS Appl. Mater. Interfaces*, 2018, **10**, 39134–39143.

45 D. V. Yakimchuk, E. Y. Kaniukov, S. Lepeshov, V. D. Bundyukova, S. E. Demyanov, G. M. Arzumanyanm, N. V. Doroshkevich, K. Z. Mamatkulov, A. Bochmann, M. Presselt, O. Stranik, S. A. Khubezhov, A. E. Krasnok, A. Alù and V. A. Sivakov, Self-organized spatially separated silver 3D dendrites as efficient plasmonic nanostructures for surface-enhanced Raman spectroscopy applications, *J. Appl. Phys.*, 2019, **126**, 233105.

46 K. Y. Lee and D. J. Mooney, Alginate: Properties and biomedical applications, *Prog. Polym. Sci.*, 2012, **37**, 106–126.

47 X. Zhao, Z. Li, Y. Deng, Z. Zhao, X. Li and Y. Xia, Facile synthesis of gold nanoparticles with alginate and its catalytic activity for reduction of 4-nitrophenol and H_2O_2 detection, *Materials*, 2017, **10**, 557.

48 J. Yang and J. Pan, Hydrothermal synthesis of silver nanoparticles by sodium alginate and their applications in surface-enhanced Raman scattering and catalysis, *Acta Mater.*, 2012, **60**, 4753–4758.

49 H. Daemi, M. Barikani and M. Barmar, Compatible compositions based on aqueous polyurethane dispersions and sodium alginate, *Carbohydr. Polym.*, 2013, **92**, 490–496.

50 J. Zhang, X. X. Wang, B. Zhang, S. Ramakrishna, M. Yu, J. W. Ma and Y. Z. Long, In Situ Assembly of Well-Dispersed Ag Nanoparticles throughout Electrospun Alginate Nanofibers for Monitoring Human Breath - Smart Fabrics, *ACS Appl. Mater. Interfaces*, 2018, **10**, 19863–19870.

51 M. H. Kim, J. J. Lee, J. B. Lee and K. Y. Choi, Synthesis of silver nanoplates with controlled shapes by reducing silver nitrate with poly(vinyl pyrrolidone) in N-methylpyrrolidone, *CrystEngComm*, 2013, **15**, 4660–4666.

52 Y. M. Park, B. G. Lee, J. Il Weon and M. H. Kim, One-step synthesis of silver nanoplates with high aspect ratios: Using coordination of silver ions to enhance lateral growth, *RSC Adv.*, 2016, **6**, 95768–95773.

53 Y. N. Wijaya, J. Kim, W. M. Choi, S. H. Park and M. H. Kim, A systematic study of triangular silver nanoplates: One-pot green synthesis, chemical stability, and sensing application, *Nanoscale*, 2017, **9**, 11705–11712.

54 M. H. Kim, D. K. Yoon and S. H. Im, Growth pathways of silver nanoplates in kinetically controlled synthesis: Bimodal *versus* unimodal growth, *RSC Adv.*, 2015, **5**, 14266–14272.

55 A. Shahzad, S. H. Bhang, E. Jung, W. S. Kim and T. Yu, Hierarchically structured 2D silver sheets with fractal network, *J. Materiomics*, 2018, **4**, 121–128.

56 J. Fang, H. You, C. Zhu, P. Kong, M. Shi, X. Song and B. Ding, Thermodynamic and kinetic competition in silver dendrite growth, *Chem. Phys. Lett.*, 2007, **439**, 204–208.

57 Z. Q. Cheng, Z. W. Li, J. H. Xu, R. Yao, Z. L. Li, S. Liang, G. L. Cheng, Y. H. Zhou, X. Luo and J. Zhong, Morphology-Controlled Fabrication of Large-Scale Dendritic Silver Nanostructures for Catalysis and SERS Applications, *Nanoscale Res. Lett.*, 2019, **14**, 89.

58 J. Hu, J. Sun, C. Bian, J. Tong and X. Shanhong, 3D Dendritic Nanostructure of Silver-Array: Preparation, Growth Mechanism and Application in Nitrate Sensor, *Electroanalysis*, 2013, **25**, 546–556.

59 J. Song, J. Hou, L. Tian, Y. Guan, Y. Zhang and X. X. Zhu, Growth of giant silver dendrites on layer-by-layer assembled films, *Polymer*, 2015, **63**, 237–243.

60 S. Wang and H. Xin, Fractal and dendritic growth of metallic ag aggregated from different kinds of γ-irradiated solutions, *J. Phys. Chem. B*, 2000, **104**, 5681–5685.

61 T. Kitanosono, K. Masuda, P. Xu and S. Kobayashi, Catalytic Organic Reactions in Water toward Sustainable Society, *Chem. Rev.*, 2018, **118**, 679–746.

62 S. Butun and N. Sahiner, A versatile hydrogel template for metal nano particle preparation and their use in catalysis, *Polymer*, 2011, **52**, 4834–4840.

63 Y. Shi, Z. Lyu, M. Zhao, R. Chen, Q. N. Nguyen and Y. Xia, Noble-Metal Nanocrystals with Controlled Shapes for Catalytic and Electrocatalytic Applications, *Chem. Rev.*, 2021, **121**, 649–735.

64 T. H. Yang, J. Ahn, S. Shi, P. Wang, R. Gao and D. Qin, Noble-Metal Nanoframes and Their Catalytic Applications, *Chem. Rev.*, 2021, **121**, 796–833.

65 S. H. Park, J. Kim, S. H. Hur, D. H. Kim and M. H. Kim, Heterophase polymer dispersion: A green approach to the synthesis of functional hollow polymer microparticles, *Chem. Eng. J.*, 2018, **348**, 46–56.

66 D. H. Kim, H. C. Woo and M. H. Kim, Room-Temperature Synthesis of Hollow Polymer Microparticles with an Open Hole on the Surface and Their Application, *Langmuir*, 2019, **35**, 13700–13710.

67 M. Arai and F. Zhao, Metal catalysts recycling and heterogeneous/homogeneous catalysis, *Catalysts*, 2015, **5**, 868–870.

68 D. H. Kim, J. H. Jeong, H. C. Woo and M. H. Kim, Synthesis of highly porous polymer microspheres with interconnected open pores for catalytic microreactors, *Chem. Eng. J.*, 2021, **420**, 127628.